Nanofabrication Process for Highly Ordered Porous Materials by the Liquid Phase Deposition Methods

Deki, Shigehito
Nakata, Akiyoshi
Miyake, Takuya
Ooka, Sachiyo
Mizuhata, Minoru

(Citation)
ECS Transactions,6(11):11-22

(Issue Date)
2007

(Resource Type)
journal article

(Version)
Version of Record

ECS Transactions, 6 (11) 11-22 (2007)
10.1149/1.2790410, ©The Electrochemical Society

Nanofabrication Process for Highly Ordered Porous Materials by the Liquid Phase Deposition Methods

Shigehito Deki and Akiyoshi Nakata, Takuya Miyake, Sachiyo Ooka, and Minoru Mizuhata

Department of Chemical Science and Engineering,
Graduate School of Engineering, Kobe University
1-1 Rokkodai-cho, Nada, Kobe 657-8501, Japan

We have studied a novel technique for the direct synthesis of two-dimensional metal oxide films with highly ordered periodic structure. TiO_2 films with highly nano-ordered architectures were directly deposited on substrates at room temperature by the liquid phase infiltration (LPI) method. 2D arrays of several kinds of metal oxide rods with diameters ranging from ca. 100 to 1000 nm are fabricated by filling the holes in a Si wafer. We summarized the various kinds of ordered structured metal oxide thin film with this method and the other techniques which have been reported that a novel soft solution process for the direct synthesis of large-area well-crystallized oxides with 1D-3D ordered periodic structure has been developed based on the LPI method. Metal oxide thin films were deposited directly into the nano-space, and thus the nano-space was completely infiltrated with metal oxide. The LPI process provides a direct fabrication route for metal oxide films with highly ordered structures, enabling nanoscale modification of optical properties of photonic crystals.

Introduction

In recent years, nanomaterials have attracted much attention since the products have been smaller in keeping with trend of density growth or integration. They have great interest scientifically and technologically because of their potential to exhibit novel properties which cannot be achieved by bulk materials. For examples, two-(2D) and three-dimensionally (3D) ordered nanomaterials have attracted much interest due to their potential applications in photonic crystals (1-4), data storage (5-8), field emission device (9-12). It is important to establish fabrication technique of materials with desired shape or size. Previously we have developed and promoted the liquid phase deposition (LPD) method as a novel aqueous solution-based process to prepare metal oxide thin films using the ligand-exchange hydrolysis of metal-fluoro complexes and the F^- consumption reaction with boric acid, aluminum metal and so on. This reaction proceeds in an aqueous solution systems. Therefore, homogeneous and/or composite thin films or multi-component thin film can be also formed only by the mixing of the objective metal ions to the treatment. It is, moreover, applied to various kinds of substrates with large surface area or complex morphologies and especially nanospace as the "Liquid Phase Infiltration Process" (13,14). Metal oxide thin films were deposited into the nanospace using this process as shown in Fig.1.

The formation mechanism of the metal oxides in solution proceeds during the

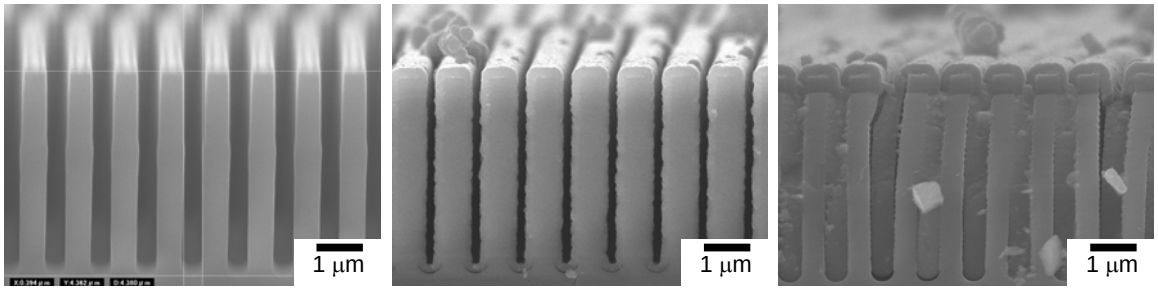

Fig. 1 SEM images of TiO_2 deposited on the Si with high aspect trench structure.

following ligand-exchange (hydrolysis) equilibrium reaction:

$$MF_x^{(x-2n)} + nH_2O = MO_n + xF^- + 2nH^+ \quad [1]$$

This equilibrium reaction [1] shifts to the right-hand side upon the addition of boric acid or aluminum metal which readily reacts with F^- ions to form more stable complex ions.

$$H_3BO_3 + 4HF \rightarrow BF_4^- + H_3O+ + 2H_2O \quad [2a]$$

$$Al + 6HF \rightarrow H_3AlF_6 + 3/2\ H_2 \quad [2b]$$

The addition of boric acid or aluminum metal accelerates the ligand-exchange hydrolysis reaction. Thin films slowly formed on the substrate at room temperature. We have adapted the LPD reaction to the fabrication of various kind of metal oxide thin films, such as titanium oxide (15, 16), vanadium oxide (17, 18), iron oxyhydroxide (19, 20), and multi-component metal oxide films (21). Using a simple method, it is possible to deposit on substrates with complex morphologies such as glass wool or porous materials. It suggests that the LPD method can be applied to preparation of metal oxide thin films with highly ordered nanostructures.

On the other hands, structures with an ordered two-dimensional (2D) pattern have attracted great attention because they are applicable to various fields. They are required suitable shape or size when they are actually put into use. For examples, they must have periodic pillar or hole structure with high aspect ratio to use as 2D photonic crystals (22, 23). They must be moth-eye structure to use as antireflection coating (24, 25), and they preferably have pointed top to use as field emission device (9-12).

There are several ways to fabricate 2D nanostructured metal oxide. For example, highly ordered hole structured Al_2O_3 has been prepared by using anodic oxidation (26). TiO_2, SnO_2 and Fe_3O_4 with micro pattern are prepared by using a seed layer process (27-29). These techniques are very useful; however, they are not adequate to fabrication of complex, desired and precision structured materials. On the other hand, an electron beam lithography (EBL) and reactive ion etching (RIE) techniques are utilized to fabricate nanopatterned substrate on resist film. In order to apply these techniques, it is easy to fabricate nanostructured silicon wafer. However metal oxides are too brittle to be handled.

In this study, we focused to design the nanostructured Si as template by using EBL and Deep-RIE in order to fabricate nanostructured metal oxides. Here, the Si structure was transcribed into polymer film. Metal oxides are deposited on the polymer film by using

LPI method and polymer film is removed. We discussed the possibility of the fabrication process of various ordered structured metal oxide thin films using various methods including the LPI process.

Experimental

Preparation of Si template A p-type single crystal silicon wafer having a thickness of 525±25μm and resistivity of 5-15Ωcm (Umesato Electronic Co., Ltd) was used. At first, high resolution positive electron beam resist ZEP520A (Nippon Zeon Co. Ltd.) was used and coated on the surface of the Si wafer by the spin coat process. Spin rotation rate was 200 rpm for 5 sec and subsequently 3000 rpm for 120 sec. Film thickness was controlled at 400 nm. Resist-coated Si wafer was baked at 180°C for 3 min. An electron beam lithography system Elionix ELS-3700 was utilized in order to draw a nano-order pattern on the wafer. An acceleration voltage and beam current were 30kV and 1 pA, respectively. Dose time of the electron was 0.2 s and 0.3 s for piller-type designed wafer and trench-type designed wafer, respectively. After e-beam process, the wafer was immersed into *o*-xylene (Nacalai Tesque Inc.) as a developer solution at 23°C with 0.1 K of error range for 50 seconds after selective exposure to a light source. Finally, the etching process was carried out by ICP dry etching method by Elionix EIS-700. SF_6 plasma was used as the etching step, and C_4F_8 and O_2 plasma were used as the overcoating deposition step. Power for ICP was 500 W and power for plate was 30 W and 0 W for SF_6 and C_4F_8 gas plasma irradiation, respectively. Standard etching condition was shown in Table.1.

Table 1. Standard etching condition

Gas	ICP power/ W	Plate Power/ W	Flow Rate/sccm	Flow Time/s
SF_6	500	30	6	9
C_4F_8	500	0	15	10

Preparation of template; poly methyl methacrylate (PMMA) In this study, polymethylmethacrylate (PMMA) and acetylcellulose was used for replication of Si morphology. Since polymethylmethacrylate (PMMA) is thermoplastic resin with low glass transition temperature, it is easy and inexpensive to cast and synthesize the template materials imprinted from the substrate. In order to fabricate polymer template, PMMA prepared by bulk polymerization method was employed. Eighty grams of methylmethacrylate monomer (MMA; Nakarai Tesque Inc.) and 1.5g of azobisisobutyronitrile (AIBN; Nacalai Tesque Inc.) were mixed in the reactor at 80°C under N_2 atmosphere for 8 or 28 minutes to obtain optimum polymer for imprinting. After polymerization reaction period, chloroform and methanol were added into the reactor sequentially. In this paper, PMMA-8 and PMMA-28 denote the ones of which polymerization times were 8 and 28 minutes, respectively.
On the other hand, acetylcellulose was used for preparation of the trench structured sample for the measurement of absolute refractive spectra. The acetylcellulose sheet was pressed on the Si substrate on which methylacetate was applied for swelling.

Preparation of stannum LPD reaction solution As a parent solution, Tin fluoride (SnF_2; Nacalai Tesque Inc.) was dissolved in distilled water. $SnO_2 \cdot nH_2O$ was precipitated by

oxidation of fluoric solution upon addition of hydrogen peroxide (H_2O_2; Santoku Chemical Inc.). After filtration of the precipitate, it was washed with distilled water repeatedly and dried at ambient temperature. Then the precipitation was dissolved in aqueous hydrofluoric acid (HF 55%, Stella Chemifa Inc.) solution at concentration of 1.5 mol dm^{-3}, and it was used as the parent solution. H_3BO_3 solution was used as an F^- scavenger in Eq [2a]. Finally, the concentrations of SnO_2-HF and H_3BO_3 in the reaction solution were controlled to 0.024 mol dm^{-3} and 0.2 mol dm^{-3} in which transparent films can be obtained.

Fabrication of SnO_2 with highly ordered periodic structure In order to deposite the hydrophobic thin layer on the Si template, C_4F_8 plasma gas was exposed on the Si template by the ICP dry etcher at final procedure of Deep-RIE process. It is important to transcribe the Si template on PMMA, these conditions are the coil power = 500 W and the flow rate of C_4F_8 = 50 sccm for 3 minute. PMMA was placed on the Si template and pressed against the Si mold at 150°C. After 10 seconds, the PMMA was cooled and peeled off and used as substrate for LPD reaction.

For the substrate, both Si wafer and transcribed PMMA and acetylcellulose were used. The substrate was suspended in the LPD reaction solution vertically. After several hours, the substrates were removed from the solution and washed with distilled water. The samples were dried at room temperature. The Aron Ceramic (Toa Gosei, Ltd.) was applied to the top surface of the SnO_2 to be supported. For the PMMA subsltrate, the PMMA was immersed in acetone and methanol (v/v=1:1) for 5min, revealing the SnO_2 film and a positive PMMA image of Si mold. As the optimum condition depends on the nano- or micropatterns of Si wafer, each condition is described below.

For measurement of reflective spectra, acetylcellulose replica film was used. The nickel backing layer was applied on the opposite side of the acetylcellulose film. Nickel film was applied by electroless plating method using nickel sulfate solution and supported by Aron Ceramics.

Characterization of fabricated Si wafers and metal oxide The surface morphology of fabricated Si wafers, PMMA and prepared metal oxide thin films with highly ordered periodic structure were observed by field emission scanning electron microscopy JEOL JEM-6335F. To prevent the surface of samples from electron charging up, thin carbon film was coated on the samples using carbon coater CC-40F (Meiwafosis Co. Ltd.). EDX elemental mapping analyzer JEOL EX-23000BU was used to elucidate the deposition of fluorocarbon on the surface of fabricated Si mold. To prevent the surface of samples from electron charging up, thin carbon film was coated on the samples using carbon coater. The glass transition temperature (T_g) of all the PMMA was determined by differential scanning calorimetry (DSC). DSC measurements were performed using a Thermo plus DSC 8230L (Rigaku Denki Co.) with a heating rate of 10 K/min in air atmosphere.

Results and Discussion

Investigation for optimal gas flow for Deep-RIE method It is important for fabrication of Si template having various structures to decide the condition. Etching conditions depend on the equipment, the substrate, mask, gases and so on (30-35). In order to optimize the condition to have smooth side wall roughness and high aspect ratio structure, gas flow rate, flow time, and etching cycle times of SF_6 and C_4F_8 gases was

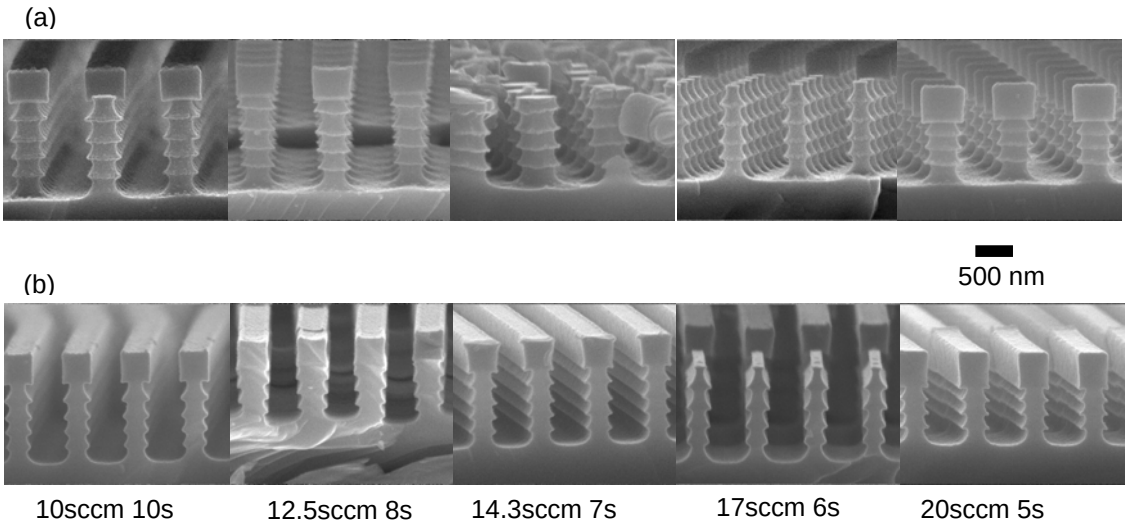

Fig. 2 SF_6 condition and SEM images of fabricated (a) Si with pillar structure and (b) Si with trench structure. Etching gas: SF_6 under ICP power: 500 W, Plate power: 30 W, Flow rate: 6 sccm, Flow time 9 sec.

parametrically changed. At first, supposing that all the SF_6 gas flowing into the chamber is involved etching process, optimum condition was investigated by changing the product value; [flow rate (sccm) × flow time (s)] of SF_6 in range of 40-100 and 3 types of condition were tried on. In this case, the C_4F_8, plasma power, chamber temperature and pressure were kept at constant condition as shown in Fig. 2. Judging from the results so far obtained, flow rate of SF_6 gas should be used within 6 sccm.

Secondary, as in the case of the condition in constant SF_6 flow, the product values of [flow rate (sccm) × flow time (s)] of C_4F_8 was changed in range of 100-300 and 3 types of condition were tried on. Fig. 3 shows the dependence of the flow rate and flow time on the surface morphology on various SF_6 and C_4F_8 supplying condition for the pillar and trench designed Si wafers based on the above results. While etching rate increased, the scallop on the Si pillar became increasingly prominent as the product values of [flow rate (sccm) × flow time (s)] of SF_6 increases. On the other hand, etching rate decreases and the scallop on the Si pillar becomes smaller as the product values of [flow rate (sccm) × flow time (s)] of SF_6 decreases. In C_4F_8, etching rate increases and the scallop on the Si pillar becomes smaller as the product values of [flow rate (sccm) × flow time (s)] of C_4F_8 increases. Therefore the scallop on the Si pillar is hardly seen, optimum condition was set as preparing Si pillar under the following condition; SF_6 flow rate = 4 sccm, flow time 10s and C_4F_8 flow rate = 10 sccm, flow time 15s.

Fabrication of Si substrate with various structures

Variation of surface morphology of Si wafer into motheye structure with the etching cycle number of SF_6 and C_4F_8 gas flow is shown in Fig. 4. In this case, each value of gas flow rate and time was larger than that for pillar structure indicated in Fig. 3; SF_6 gas flow rate and time are 4 sccm and 7.5 s, and C_4F_8 gas flow rate and time are 10 sccm and 25 s. As increasing number of etching times, the Si substrate is etched not depth direction but side direction. It is considered that generated F radical in chamber attacks the edge of resist mask than Si substrate.

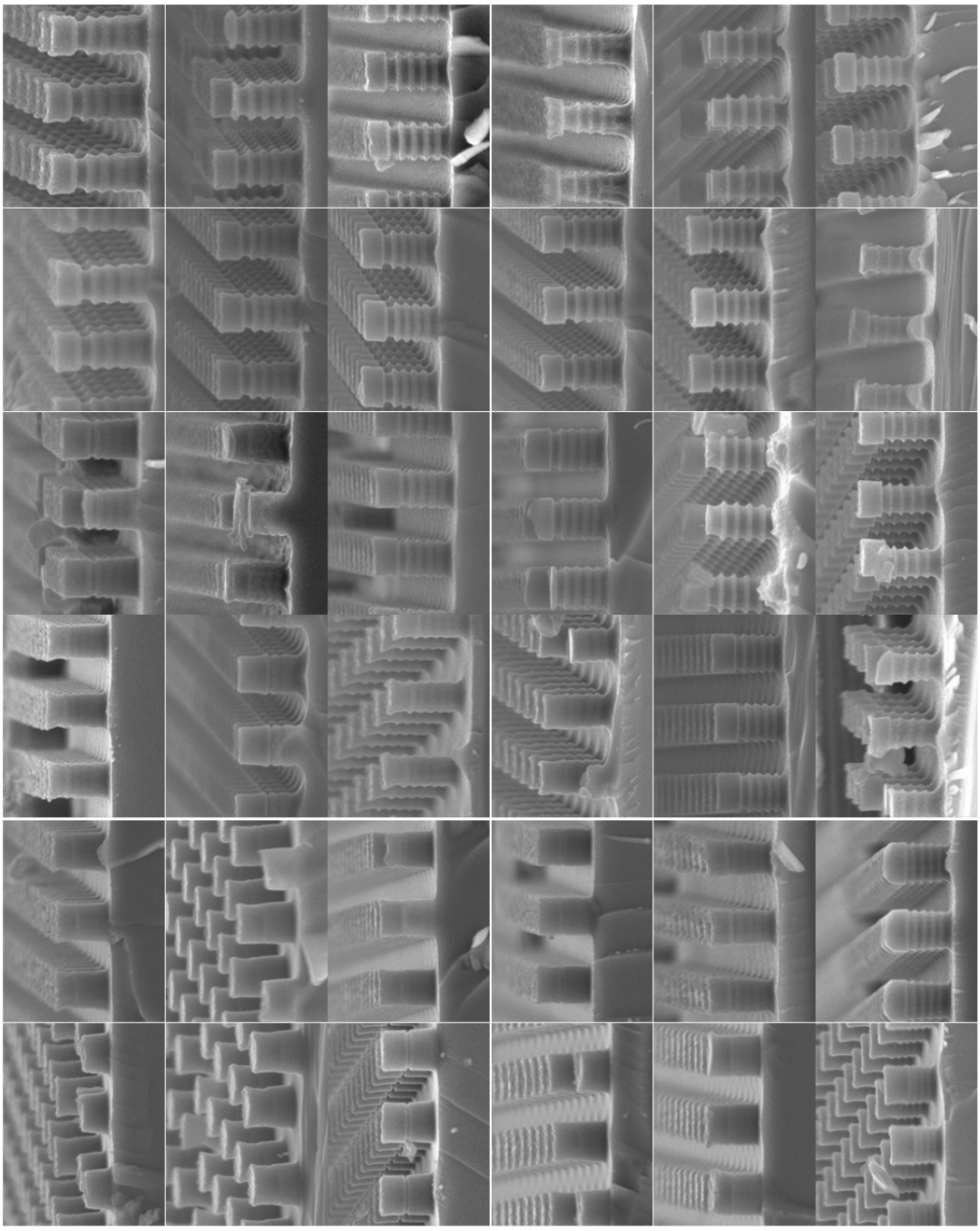

Fig. 3 C_4F_8 and SF_6 flow condition and corresponding SEM images of fabricated Si with pillar structure.

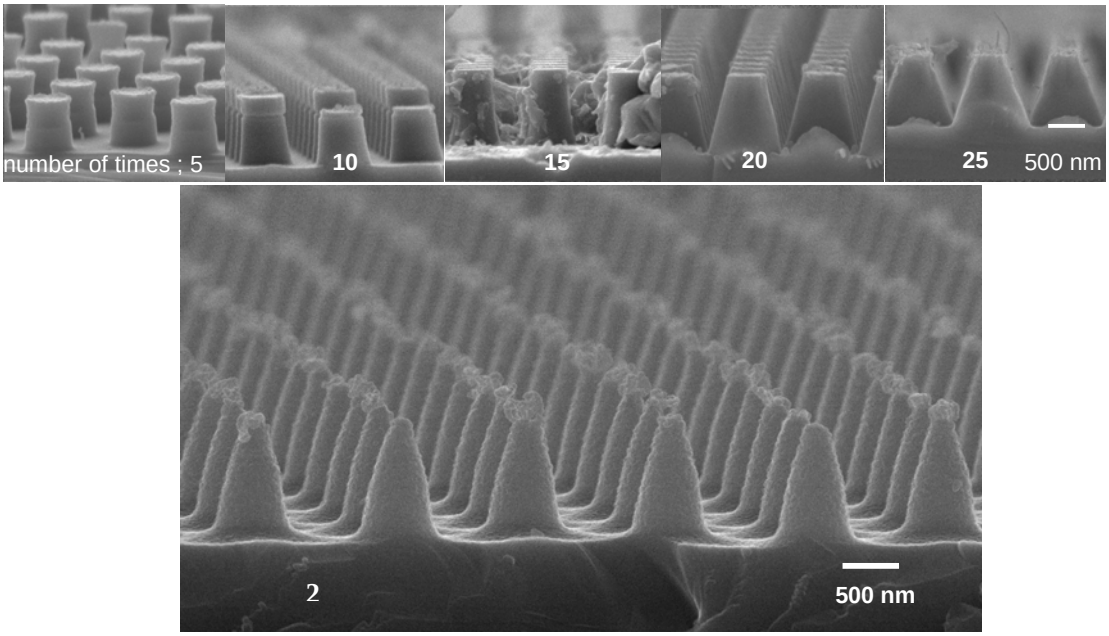

Fig. 4 Prepared Si substrates with moth eye structure.

We also tried to fabrication the trench structure with high aspect ratio. Variation of the structure of Si trench structure with the etching cycle number of SF_6 and C_4F_8 gas flow is shown in Fig. 5. As increasing number of etching times, the Si substrate is etched for depth direction and its aspect ratio increases.

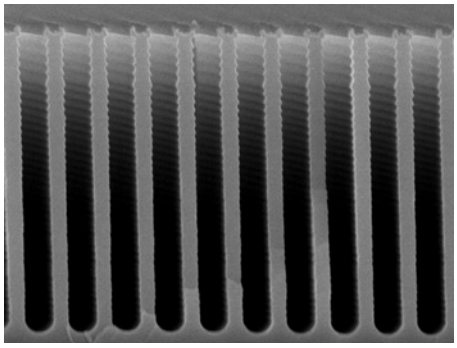

Fig. 5 Prepared Si substrates with trench structure.

As described above, specific conditions for each process were empirically found in various samples. We found that the scallop shape was easily found in most cases that SF_6 flow rate was more than 20 sccm. In Fig.6, the SEM image of various kinds of etched Si wafer designed by the same condition. In this case, SF_6 gas flow was set in 20 sccm and 4 s and C_4F_8 gas flow was set in 50 sccm and 5 s. For all cases, there is no scallop shape and good reproducibility. To fabricate the deeply dug structure, the flow time can be short because of protect from the erosion of side wall by etching gas, although the repetition time might increased. This condition was extended to not only periodic structural design but also any drawing image such as Fig.6f.

We tried to fabrication the trench structure with high aspect ratio, as shown in Fig.7. As increasing number of etching times, the Si substrate is etched for depth direction and its aspect ratio increases up to ca 32.

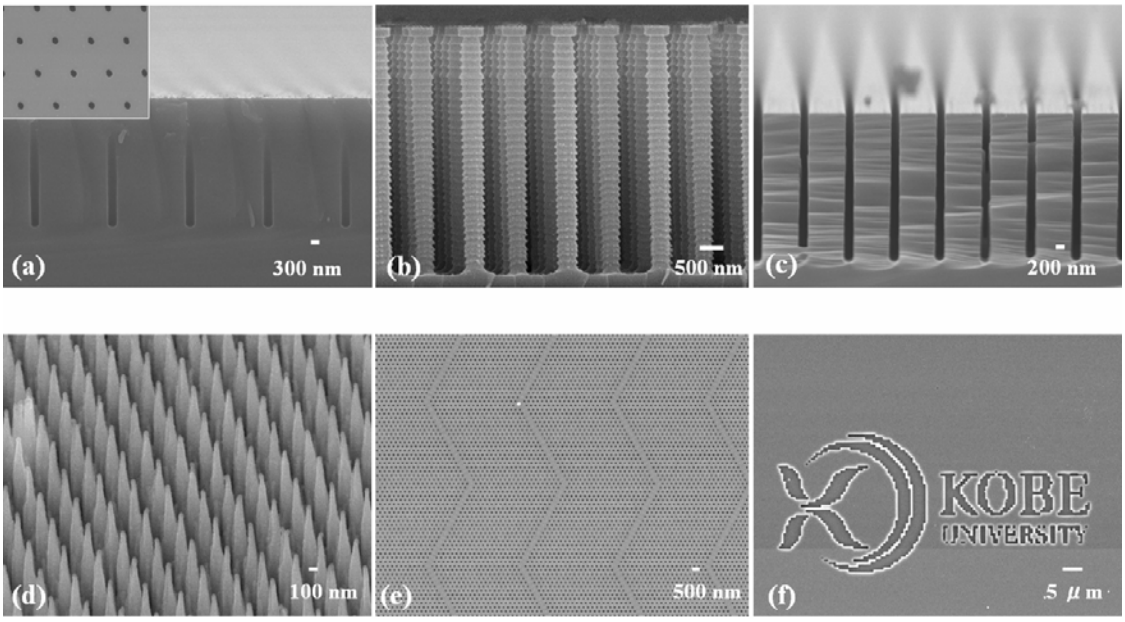

Fig. 6. SEM images of fabricated Si with various structure.

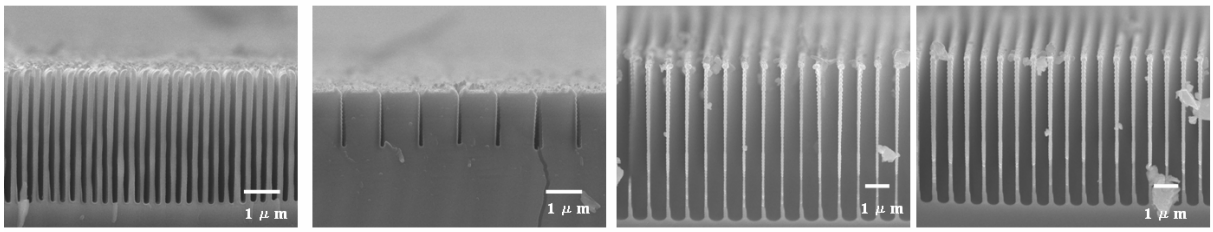

Fig. 7. SEM images of fabricated Si with ultra-high aspect ratio trench structure.

Optimum condition of PMMA for imprinting of fabricated Si pillar

According to DSC measurement of synthesized PMMA, each glass transition temperature; T_g remains within 180°C in air condition, therefore the imprinting temperature was set 50°C higher than each T_g. In this case, the fluorocarbon was deposited in order to improve the liftoff condition from Si surface (36). Fig. 8 shows SEM images of Si template and PMMA transcribed the Si template. In this case, the diameter of Si pillar is 600 nm. There is no broken Si pillar rod in the PMMA-8 hole and replica form of Si template was prepared successfully as shown in Fig. 8(C-1). However, in the case of using PMMA-28, the Si pillar rods remained in the PMMA matrix as shown in Fig. 7c. It is suggested that the shape of pillared Si wafer was transcribed into PMMA, however, the hardness of PMMA-28 caused a fail of PMMA liftoff from Si substrate. PMMA-28 has high degree of polymerization in comparison with PMMA-8, therefore its flexibility or hardness is not suitable to transcribing.

Dependence of diameter of Si pillar rod on the transcribe condition also. In the case of diameter of 400 nm, most part of Si pillars was successfully transcribed. However, Si rod was remained in a little part of PMMA-8. In the case of diameter of 200 nm, there are small trace points made by the top of Si pillar. From these results, we tried to prepare the metal oxide thin films using Si pillar with the diameter of 500 nm and PMMA-8 as template polymer in the following experiment.

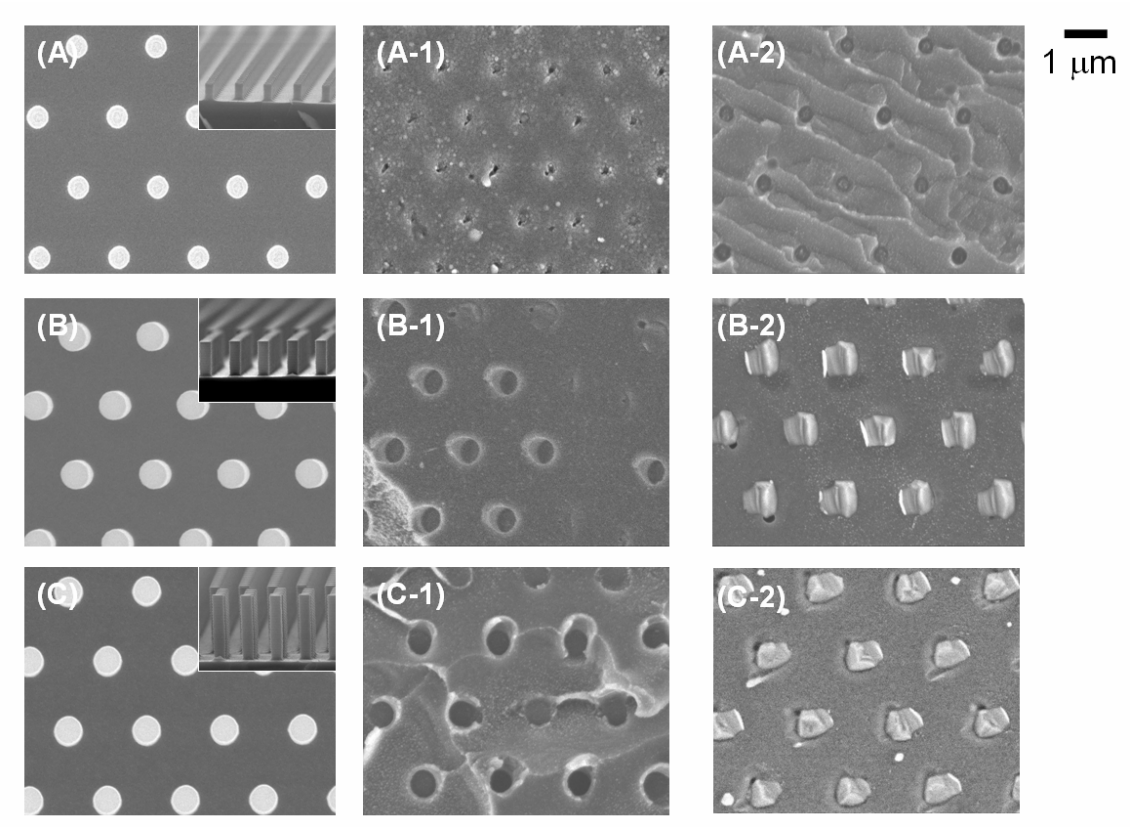

Fig.8 SEM images of Si pillar and transcribed PMMA. Diameters of hole: (A) 250 nm, (B)500 nm, and (C)1μm. PMMA (1)PMMA-8 and (2) PMMA-28.

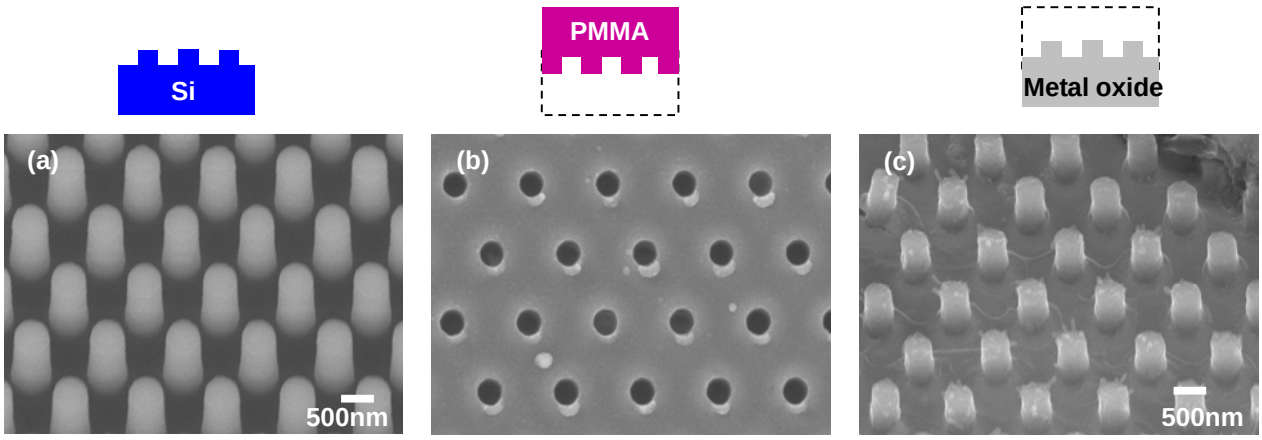

Fig. 9 SEM images of transcribing scheme of 2D ordering structure of the samples. (a) Template (Si pillar), (b) PMMA of transferred template, (c) Nanostructured SnO_2

Fabrication of highly structure ordered periodic structure Fig. 9 shows fabrication scheme of nanostructured metal oxide. Figure 9c shows the FE-SEM image of SnO_2 pillar array. SnO_2 exhibit hexagonal array of pillar on long length scales, with the same periodicity as the pillar on the Si substrate used as a template. Some amount of shrinkage

was seen because the PMMA shrinks at heat treatment as shown in Fig.9b. The distance and diameter were shortened by the volume change of the sample. However, its topological condition did not change during this procedure. Infiltration condition was confirmed using periodic structured Si substrate. The Si pillar was buried in the PMMA after transcription from Si to PMMA. The author considers that the PMMA had the nature of heat-shrinkable that it shrinks at cooling, the stress generated when peeling off concentrates the Si root, the Si pillar was broken (37). In case of using replica method, the Si was broken at root or the replica could not keep its structure because the replica is soft (38).

Consequently, EBL and Deep-RIE process are useful to fabricate a nanostructured template for the liquid phase deposition process.

Conclusions

We have fabricated motheye, high aspect pillar, and trench structures as the template materials for the liquid phase infiltration process. By using PMMA and ceramic glue, the Liquid Phase Infiltration method found to be applied to transcribe template with various metal oxide. We established the transcription method for LPI process besides the process using 3D inversed opal which has nanometer ordered structure(39) and 1D graded composition thin films and so on (40). Recently, we applied to molecular range ordered solution process. Monodispersed TiO_2 nanoparticles were synthesized by the LPD process controlling the size and reactivity of metal-fluoro complex, using

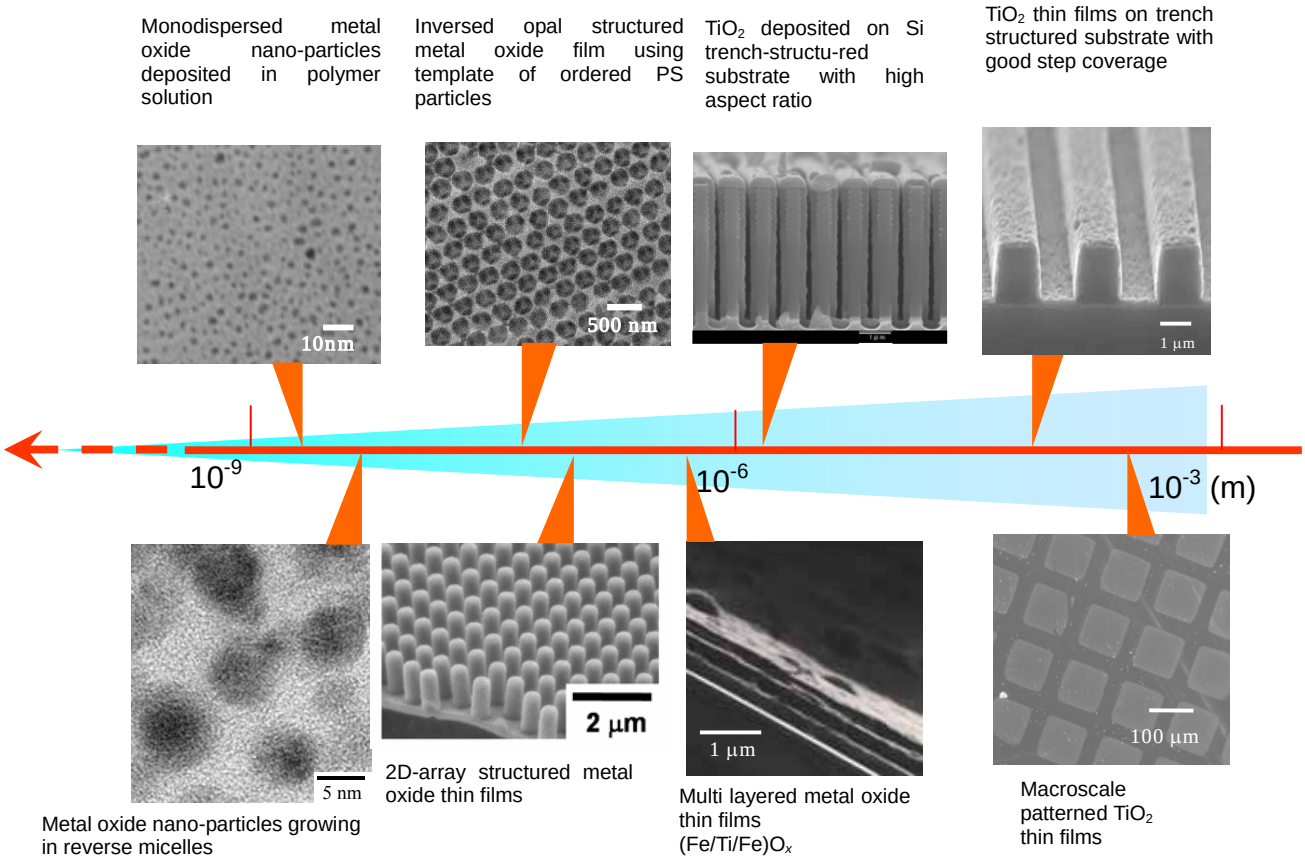

Scheme 1. Ordering structured metal oxide fabricated by the Liquid Phase Deposition method.

polyethyleneglycol (41). The present method represents a simple route for the production of crystalline metal oxide nanoparticles with potentially interesting applications at ambient condition. Here we summarized the multi-ordered fabrication applied to the LPD process as shown in Scheme 1. It is expected to the extension toward the molecular size ordered materials using molecular imprinting (42, 43).

Acknowledgments

This study was supported by Grant-in-Aid for Scientific Research (A) Nos. 15205026, 19205029 from Japan Society for the Promotion of Science and Priority Area No. 16080211 from Ministry of Education, Culture, Sports, Science and Technology of Japan.

References

1. E. Yablonovitch, *Phys. Rev. Lett*., **58**, 2059 (1987).
2. V. V. Poborchii, *J. Appl. Phys*, **91**, 3299 (2002).
3. F. Pommereau, L. Legouezigou, G. H. Duan, B. Lombardet, *J. Appl. Phys*., **95**, 2242 (2004).
4. H. C. Guo, D. Nau, A, Ranke, H, Giessen, *Appl. Phys. B*, **81**, 271 (2005).
5. I. Soten, H. Miguez, S. M. Yang, S. Petrov, N. Coombs, N. Tetreault, N. Matsuura, H. E. Ruda and G. A. Ozin, *Adv. Funct. Mater.*, **12**, 71 (2002).
6. T. Aoki, M, Kuwabara, *Appl. Phys. Lett.*, **27**, 2580 (2004).
7. T. Aoki, M. Kondo, K. Kurihara, N. Kamehara, M. Kuwabara, *J. J. Appl. Phys*., **45**, 350 (2006).
8. J.E. Jang, S. N. Cha, Y. Choi, G. A. J. Ameratunga, D. J. Kang, *Appl. Phys. Lett*., **87**,263103 (2005).
9. A. G. Rinzler, J. H. Hafner, P. Nikolaev, L. Lou, R. E. Smalley, *Science*, **269**, 1550 (1995).
10. M. Noh, J. Thiel, D. C. Johnson, *Science*, **270**, 1181 (1995).
11. K. Yu, Y. Zhang, R. Xu, S. Ouyang, D. Li, L. Luo, Z. Zho, J. Ma, *Mater. Lett*., **59**,1866 (2005).
12. Y. Zhang, K. Yu, G. Li, D. Peng, Q. Zhang, F. Xu, W. Bai, *Mater. Lett*., **60**,3109 (2006).
13. S. Deki, S. Iizuka, A. Horie, M. Mizuhata and A. Kajinami, *Chem. Mater*., **16**, 1747 (2004).
14. S. Deki, S. Iizuka, A. Horie, M. Mizuhata and A. Kajinami, *J. Mater. Chem*., **14**, 3127 (2004).
15. S. Deki, Y. Aoi, O. Hiroi and A. Kajinami, *Chem. Lett*., 33 (1996)
16. S. Deki, Y. Aoi, Y. Asaoka, A. Kajinami and M. Mizuhata, *J. Mater. Chem*., **7**, 733 (1997).
17. S. Deki, Y. Aoi, Y. Miyake, A. Gotoh and A. Kajinami, *Mater. Res. Bull.*, **31**, 1399 (1996).
18. S. Deki, Y. Aoi and A. Kajinami, *J. Mater. Sci.*, **32**, 4269 (1997).
19. S. Deki, Y. Aoi, J. Okibe, H. Yanagimoto, A. Kajinami and M. Mizuhata, *J. Mater. Chem.*, **7**, 1769 (1997).
20. S. Deki, N. Yoshida, Y. Hiroe, K. Akamatsu, M. Mizuhata and A. Kajinami, *Solid State Ion.*, **151**, 1 (2002).
21. S. Deki, Y. Aoi, H. Yanagimoto, K. Ishii, K. Akamatsu, M. Mizuhata and A. Kajinami, *J. Mater. Chem*., **6**, 1879 (1996).

22. V. Mizeikis, S. Juodkazis, J. Y. Ye, A. Rode, S. Matsuo, H. Misawa, *Thin. Solid. Films*, **438**,445 (2003).
23. V. V. Poborchii, *Appl. Phys. Lett*., **75**,3276 (1999).
24. H. Toyota, K. Takahara, M. Okano, T. Yotsuya, H. Kikuta, *J. J. Appl. Phys.*, **40,**747 (2001**)**
25. D. H. Macdonald, A. Cuevas, M. J. Kerr, C. Samundsett, D. Ruby, *Solar. Energy,* **76**,277(2004).
26. I. Mikulskas, S. Juodkazis, R. Tomasiunas, J. G. Dumas, *Adv. Mater*., **13**,1574 (2001).
27. N. Shirahata, Y. Masuda, T. Yonezawa, K. Koumoto, *Langmuir,* **18**,10379 (2002).
28. T. Nakanishi, Y. Masuda, K. Koumoto, *J. Crystal. Growth*, **284**,176 (2005).
29. Y. Masuda, S. Ieda, K. Koumoto, *Langmuir,* **19**,4415 (2003).
30. Y. Chinzei, Y. Feurprior, M. Ozawa, T. Kikuchi, K. Horioka, *J. Vac. Sci. Tech. A*, ,**18**,158(2000).
31. A. Sankaran, M. J. Kushner, *J. Appl. Phys*., **97,**023307(2005).
32. S. Trellenkamp, J. Moers, A. V. Hurt, P. Kordos, *Microelectronic. Engineering*, **67**,376 (2003).
33. J. Li, A. Q. Liu, Q. X. Zhang, *Sensor and Actuators A*,**125**,494 (2006).
34. L. Zhou, F. Luo, M. Cao, *Thin Solid Films*, **489**,229 (2005).
35. H. C. Liu, Y. H. Lin, W. Hsu, *Microsystem Technologies*, **10**, 29(2003)
36. G. Y. Jung, Z. Li, W. Wu, Y. Chen, D. L. Olynick, S. Y. Wang, W. M. Tong, *Langmuir*, **21,**1158 (2005).
37. Y. Hirai, S. Yoshida, N. Takagi, Y. Tanaka, H. Yabe, K. Sasaki, *J. J. Appl. Phys*. **42**,3863 (2003).
38. L. Xia, G. M. Whitesides, *Angew. Chem. Int. Ed*., **37**, 550 (1998).
39. S. Iizuka, S. Ooka, A. Nakata, M. Mizuhata, S. Deki, *Electrochim. Acta.*, **51**, 802 (2005).
40. S. Deki, S. Iizuka, K. Akamatsu, M. Mizuhata, and A. Kajinami, J. Am. Ceram. Soc., 88, 731 (2005).
41. S. Deki, A. Nakata, and M. Mizuhata, *ECS Transactions*, **3(9)**, 29 (2006).
42. L. A. Feng, Y. J. Liu, J. M. Hu, *Langmuir*, **20**, 1786 (2004).
43. M. Tatemichi, M. Sakamoto, M. Mizuhata, S. Deki, and T. Takeuchi, *J. Am. Chem. Soc.*, in press.